International Journal of Physics and Mathematics

E-ISSN: 2664-8644
P-ISSN: 2664-8636
IJPM 2025; 7(2): 60-64

www.physicsjournal.net
Received: 27-05-2025
Accepted: 30-06-2025

Kasukurthy Ramarao
Department of Physics, St. Mary's Group of Institutions, Deshmukhi, Yadadri Bhuvanagiri, Telangana, India

N Hari Kumar
Department of Physics, St. Mary's Group of Institutions, Deshmukhi, Yadadri Bhuvanagiri, Telangana, India

Corresponding Author:
Kasukurthy Ramarao
Department of Physics, St. Mary's Group of Institutions, Deshmukhi, Yadadri Bhuvanagiri, Telangana, India

Synthesis and structural characterization of magnesium-substituted Ni-Zn ferrites fabricated through the innovative citrate-gel auto-combustion technique

Kasukurthy Ramarao and N Hari Kumar

DOI: https://doi.org/10.33545/26648636.2025.v7.i2a.126

Abstract
Ferrite nanoparticles, characterized by the chemical formula $Ni_{0.2}Mg_xZn_{0.8-x}Fe_2O_4$ (where x ranges from 0.0 to 0.8 in increments of 0.2), were successfully synthesized using the innovative Citrate-Gel Auto Combustion method at a low temperature. The resulting powders underwent sintering at 500°C for 4 hours in air, followed by comprehensive characterization through X-ray Diffraction (XRD) and Scanning Electron Microscopy (SEM) combined with Energy Dispersive Spectroscopy (EDS). The XRD analysis unequivocally confirmed the presence of a single cubic spinel structure in the prepared samples. The crystallite sizes (D) ranged impressively from 25 to 74 nm, showcasing the impact of synthesis conditions. Notably, as magnesium substitution increased, a discernible trend was observed: the lattice parameter (a) decreased while the X-ray density (dx) increased. The surface morphology, meticulously examined via SEM, provided further insight, while EDS offered a detailed analysis of the elemental composition. The compelling results derived from this study can be effectively explained by the interplay between composition and crystallite size, underscoring the significance of these findings in the field of ferrite material research.

Keywords: Ferrites, citrate-gel auto combustion method, XRD, SEM, eds

1. Introduction
Nanomaterials have been integral to human innovation for centuries; however, the revelation of certain materials as nano-structured is a relatively recent development, enabled by sophisticated tools that can unravel information at the nanoscale. The properties of ferrites are not only complex but also highly sensitive to factors such as synthesis methods, conditions, parameters, and the nature and type of substitutions, as well as cation distribution. Ferrites play a crucial role in technological advancement and are extensively utilized in high-frequency applications. Their remarkable compositional variability is one of their standout advantages. Ferrite nanoparticles, in particular, are a significant class of magnetic materials, given their wide array of applications. What truly sets them apart is the striking difference in properties between nanomaterials and their bulk counterparts. The growing interest in ferrite nanoparticles is driven by their exceptional physical and chemical properties and their vast potential for groundbreaking technological applications, including high-density magnetic storage, electronic and microwave devices, sensors, and magnetically guided drug delivery. The versatility and capability of ferrite nanoparticles position them at the forefront of modern technology and innovation.

The transport properties of nanoparticles are primarily determined by the grain boundaries rather than the grains themselves, highlighting the critical role of these interfaces in their performance. To achieve optimal molecular mixing, chemical homogeneity, and precise stoichiometric control, a variety of innovative chemical methods have been employed in the synthesis of spinel ferrites. Notably, several researchers have successfully synthesized Ni-Zn-Mg ferrites using an array of advanced techniques, including the refluxing process, ceramic method, hydrothermal method, combustion method, co-precipitation method, reverse micelle process, and spark plasma sintering. Other noteworthy approaches, such as the microemulsion method and ball milling, further demonstrate the diversity of strategies available. In this study, we present our findings on the synthesis and structural characterization of Ni-Mg-Zn ferrites through a groundbreaking non-conventional citrate gel auto- combustion method. Our results

underline the effectiveness of this approach in producing high-quality ferrites with tailored properties.

2. Experimental

2.1 Synthesis

The synthesis of Ni-Mg-Zn ferrite particles, represented by the chemical formula $Ni_{0.2}Mg_xZn_{0.8-x}Fe_2O_4$ (where x varies from 0.0 to 0.8 in increments of 0.2), was successfully executed using the innovative Citrate-Gel Auto Combustion method. The process utilized high-purity raw materials, including Nickel Nitrate, Magnesium Nitrate, Zinc Nitrate, Ferric Nitrate, Citric Acid, and Ammonia, all sourced from SDFCL at a purity of 99%. To begin, precise amounts of the metal nitrates and citric acid were dissolved in a minimal quantity of distilled water, resulting in a clear, homogeneous solution. Citric acid played a crucial role as a chelating agent, ensuring an even distribution of metal ions throughout the mixture. The solution was carefully stirred until fully homogeneous and then heated to 80 °C using a hot plate magnetic stirrer. Subsequently, the pH was meticulously adjusted to 7 by the addition of ammonia, leading to the formation of a stable sol. The next step involved evaporating the solution to dryness at approximately 180 °C while maintaining continuous stirring on a hot plate. This process triggered a rapid, flameless auto-combustion reaction, characterized by the release of substantial amounts of gas, ultimately yielding a burned powder. This powder was then finely ground using an agate mortar and pestle, resulting in a high-quality ferrite powder. Finally, the ground ferrite was calcined in air at 500 °C for 4 hours, followed by cooling to room temperature, which facilitated the successful formation of the desired spinel phase. This meticulous process underscores the effectiveness and precision of the Citrate-Gel Auto Combustion method in synthesizing advanced ferrite materials.

2.2 Characterization

The investigation of the Ni-Mg-Zn ferrite system was conducted using a Bruker D8 advanced X-ray diffractometer with a Cu Kα radiation source (λ = 1.5405 Å). This analysis effectively demonstrated the single-phase nature and nano-phase formation at room temperature, with continuous scanning executed across a temperature range of 10 °C to 80 °C. To further enhance our understanding of the materials, Scanning Electron Microscopy (SEM) provided detailed insights into the microstructure of the prepared samples, while Energy Dispersive Spectroscopy (EDS) delivered precise elemental compositional analysis for each sample. This comprehensive approach ensures robust and reliable findings for the Ni-Mg-Zn ferrite system.

3. Results and Discussions

3.1 XRD Analysis

The X-ray diffraction pattern for all samples, as shown in Fig. 1, clearly validates the formation of a pure single-phase cubic spinel structure, devoid of any impurity peaks. Notably, the most intense reflection across all samples corresponds to the (311) peak, underscoring the consistency of the structure. Additionally, the crystalline size of each sample was meticulously calculated from the half-width at half maximum (HWFM) of the (311) reflection peak in the XRD pattern, utilizing Debye-Scherrer's formula [15]. This robust analysis reinforces the reliability of the results.

Scherrer Formula

$$Crystalline\ size\ of\ the\ sample\ \ \boldsymbol{D = \frac{0.91\lambda}{\beta\ cos\theta}}$$

Where λ =wavelength of the X-ray used
B= Full Width Half Maxima (FWHM) in radians.
θ = peak position.
The lattice parameter(a) of the sample was calculated by the formula

$$a = d * (h^2 + k^2 + l^2)^{1/2}$$

Where a Lattice Constant
(hkl) Are the Miller Indices
d = inter planner spacing,

X-ray densit $dx = \frac{nM}{a^3 N}[g/cm^3]$ [16]

Where M = molecular weight of the sample
n =number of molecules in a unit cell of the spinel lattice.
a =lattice parameter, and N is the Avogadro number.

The Volume of the Unit Cell **V a³**

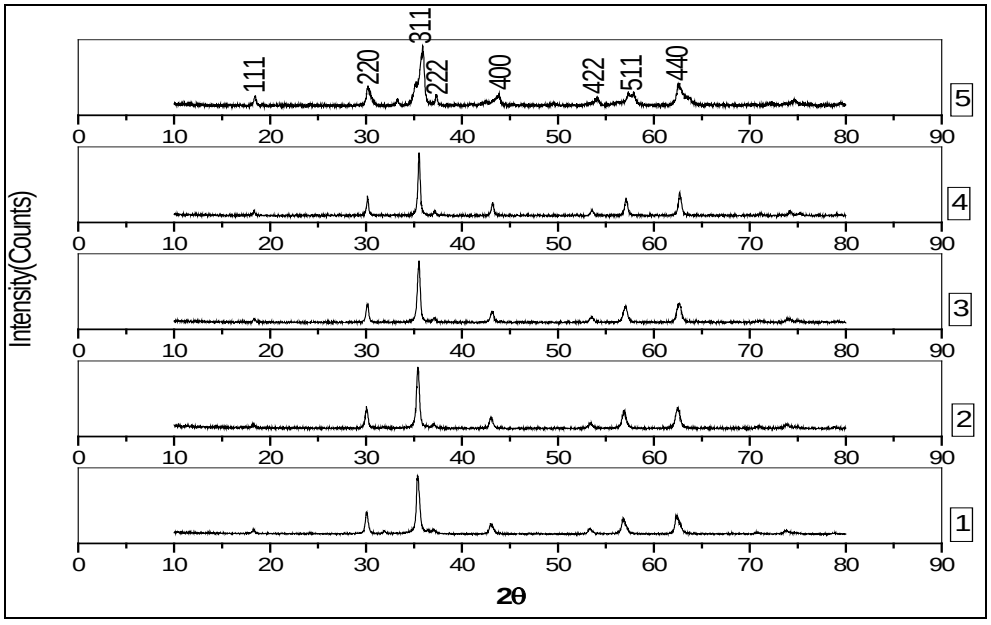

Fig 1: XRD Pattern of Ni-Mg-Zn Ferrites

Values of Crystallite size, lattice parameter, X-ray density, and volume of all the samples were given in Table 1.

Table 1: Crystalline size, Lattice Parameter, X-ray density &Volume

S. no	Sample	Mol. Wt. (gm/mol)	Crystallite size(nm)	Lattice constant (A°)	X-ray density (gm/cc)	Volume $(A°)^3$
1	$Ni_{0.2}Zn_{0.8}Fe_2O_4$	240.736	55.28	8.408	5.350	594.187
2	$Ni_{0.2}Cu_{0.2}Zn_{0.6}Fe_2O_4$	240.369	55.59	8.407	5.361	593.975
3	$Ni_{0.2}Cu_{0.4}Zn_{0.4}Fe_2O_4$	240.003	55.77	8.387	5.382	589.746
4	$Ni_{0.2}Cu_{0.6}Zn_{0.2}Fe_2O_4$	239.636	73.36	8.380	5.387	588.270
5	$Ni_{0.2}Cu_{0.8}Fe_2O_4$	239.269	25.14	8.314	5.508	574.478

The data presented in the table clearly demonstrates that the crystallite size of the prepared samples varies between 25.13 nm and 73.35 nm. Notably, we observe a significant decrease in lattice parameters as Cu concentration increases, a trend that aligns with Vegard's law [17]. This reduction in crystallite size can be effectively explained by examining the relative ionic radii of Cu and Zn ions. The ionic radius of Mg^{2+} (1.60 Å) is greater than that of Zn^{2+} (0.74 Å), which plays a crucial role in influencing crystallite size. Furthermore, the X-ray density of the prepared samples shows a marked increase with elevated Mg concentration. This enhancement is attributable to the direct relationship between X-ray density, molecular weight, and lattice parameters. As we see a decline in lattice parameters, it logically follows that X-ray density will rise. Additionally, since the volume of the unit cell is contingent on the lattice parameters, a decrease in these parameters leads to a corresponding decrease in the volume of the unit cell [18]. These observations collectively underscore the intricate relationships between ionic radii, crystallite size, and structural characteristics, reinforcing the significance of our findings.

3.2. SEM Analysis

Microstructural analysis of the prepared samples was performed using Scanning Electron Microscopy (SEM), and the resulting micrographs are showcased in Figure 2. These images compellingly demonstrate a nearly uniform grain distribution, along with distinct clusters between the particles. Remarkably, the grain sizes of the samples are confined to the nanometer range, characterized by a spherical shape and a narrowly defined size distribution [19]. Notably, the SEM images indicate a clear trend: as the concentration of magnesium increases, the grain size generally expands, except for the specific case of x=0.8. This finding aligns seamlessly with the results obtained from the X-ray Diffraction (XRD) analysis, reinforcing the significance of our observations.

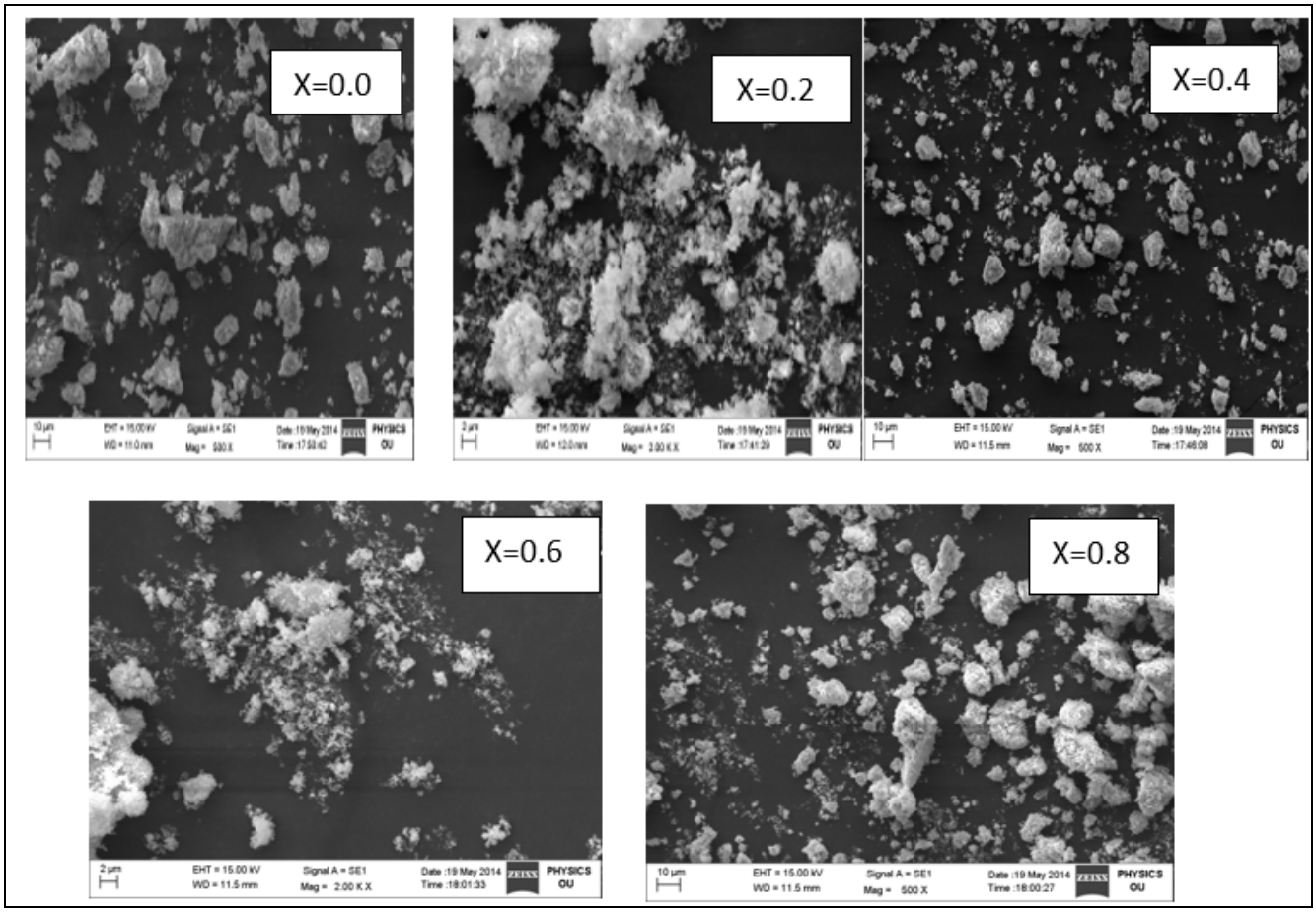

Fig 2: SEM Micrographs of Ni-Mg-Zn Nano ferrites

3.3. EDS Analysis

An Energy Dispersive Spectrometer was used for the elemental analysis of all the prepared ferrites with different compositions. The EDS spectra of all prepared samples are shown in Figure 3. The compounds show the presence of Mg, Zn, NI, Fe, and O without precipitating cations [20-21].

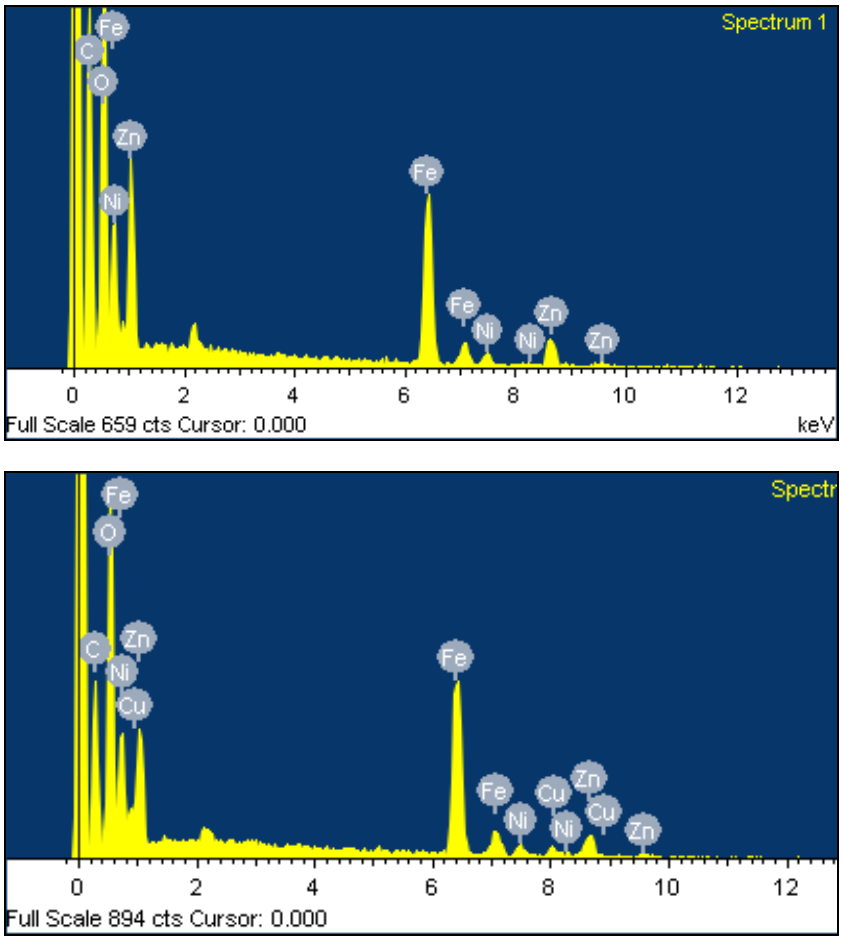

Fig 3: EDS Spectra of Ni-Mg-Zn Nano Ferrites

4. Conclusions

The X-ray diffraction pattern of the prepared samples compellingly confirms the formation of a single-phase cubic spinel structure. Notably, the substitution of magnesium (Mg) in the nickel-zinc (Ni-Zn) ferrite system leads to a significant decrease in the lattice parameter, while the crystallite size of the samples impressively ranges from 25 to 74 nm. Furthermore, the X-ray density of the samples demonstrates a marked increase with Mg substitution, highlighting the enhanced material properties. Scanning electron microscope (SEM) micrographs reveal that despite the various compositions, the particle morphology remains consistent, characterized by substantial agglomeration. This suggests a robust and uniform structural integrity across the samples.

5. Acknowledgements

The authors are very grateful to Dean, Principal St. Mary's group of institutions Hyderabad, Deshmukhi, Yadadri Bhongiri, Telangana-508512, India, for their encouragement in research work.

6. References

1. Patel SK, Kuriachen B, Kumar N, Nateriya R. The slurry abrasive wear behaviour and microstructural analysis of A2024-SiC-$ZrSiO_4$ metal matrix composite. Ceram Int. 2018;44(6):6426-6432. https://doi.org/10.1016/j.ceramint.2018.01.037
2. Kumar N, Shukla A, Kumar N, Choudhary RNP, Kumar A. Structural, electrical, and multiferroic characteristics of lead-free multiferroic: $Bi(Co_{0.5}Ti_{0.5})O_3$-$BiFeO_3$ solid solution. RSC Adv. 2018;8:36939-36946. https://doi.org/10.1039/C8RA02306A
3. Patel SK, Kuriachen B, Kumar N, Nateriya R. The slurry abrasive wear behaviour and microstructural analysis of A2024-SiC-$ZrSiO_4$ metal matrix composite. Ceram Int. 2018;44(6):6426-6432. https://doi.org/10.1016/j.ceramint.2018.01.037
4. Prasad SAV, Deepty M, Ramesh PN, Prasad G, Srinivasarao K, Srinivas C, *et al*. Synthesis of MFe_2O_4 ($M = Mg^{2+}$, Zn^{2+}, Mn^{2+}) spinel ferrites and their structural, elastic and electron magnetic resonance properties. Ceram Int. 2018;44(9):10517-10524. https://doi.org/10.1016/j.ceramint.2018.03.070
5. Thansanga L, Shukla A, Kumar N, Choudhary RNP. Studies of structural, electrical and ferroelectric characteristics of gadolinium and yttrium modified bismuth ferrite. Mater Chem Phys. 2021;263:124359. https://doi.org/10.1016/j.matchemphys.2021.124359
6. Agarwal R, Agrawal NK, Kumar N, *et al*. A review on heat transfer modulation using experimental approach. Trans Indian Inst Met. 2022;75:2997-3005. https://doi.org/10.1007/s12666-022-02710-6
7. Kumar N, Shukla A, Kumar N, Agarwal R, Choudhary RNP. Eco-friendly $Bi(Ni_{2/5}Ti_{2/5}Fe_{1/5})O_3$ nanoceramics: Synthesis, dielectric and impedance studies. Ceram Int. 2021;47(15):22147-22154. https://doi.org/10.1016/j.ceramint.2021.04.237
8. Sharma H, Rana S, Singh P, Hayashi M, Binder WH, Rossegger E, *et al*. Self-healable fiber-reinforced vitrimer composites: overview and future prospects. RSC Adv. 2022;12:32569-32590. https://doi.org/10.1039/d2ra05103f
9. Kumar N, Shukla A, Kumar N, Agarwal R, Choudhary RNP. Response/refutation to the comments and concerns

of Correspondence on published papers: Ceramics International 45, 822 (2019) and Ceramics International 47, 22147 (2021). Ceram Int. 2022;48:8789-8792. https://doi.org/10.1016/j.ceramint.2021.12.237
10. Patel SK, Kuriachen B, Kumar N, Nateriya R. The slurry abrasive wear behaviour and microstructural analysis of A2024-SiC-$ZrSiO_4$ metal matrix composite. Ceram Int. 2018;44:6426-6432.
11. Khirade PP, Birajdar SD, Raut A, Jadhav K. Effect of Fe substitution on phase transformation, optical, electrical and dielectric properties of $BaTiO_3$ nanoceramics synthesized by sol-gel auto combustion method. J Electroceramics. 2016;37:110-120. https://doi.org/10.1007/s10832-016-0044-z
12. Singha KK, Singh PP, Narzary R, Mondal A, Gupta M, Sathe VG, *et al*. Crystal structure, Raman spectroscopy and optical property study of Mg-doped SnO_2 compounds for optoelectronic devices. Crystals. 2023;13:932. https://doi.org/10.3390/cryst13060932
13. Narzary R, Dey B, Rout S, Mondal A, Bouzerar G, Kar M, *et al*. Influence of K/Mg co-doping in tuning room temperature d^0 ferromagnetism, optical and transport properties of ZnO compounds for spintronics applications. J Alloys Compd. 2023;934:167874. https://doi.org/10.1016/j.jallcom.2022.167874
14. Narzary R, Dey B, Chouhan L, Kumar S, Ravi S, Srivastava SK. Optical band gap tuning, zero dielectric loss and room temperature ferromagnetism in (Ag/Mg) co-doped SnO_2 compounds for spintronics applications. Mater Sci Semicond Process. 2022;142:106477. https://doi.org/10.1016/j.mssp.2022.106477
15. Narzary R, Dey B, Sen S, Parida BN, Mondal A, Ravi S, *et al*. Influence of Na/Mg co-doping in tuning microstructure, transport, optical, and magnetic properties of TiO_2 compounds for spintronics applications. Magnetochemistry. 2022;8(11):150. https://doi.org/10.3390/magnetochemistry8110150
16. Singha KK, Mondal A, Gupta M, *et al*. Impact of Sb/Ag co-doping on SnO_2's optical, transport, and crystallographic properties for optoelectronic devices. J Mater Sci Mater Electron. 2023;34:1421-1433. https://doi.org/10.1007/s10854-023-10854-4
17. Brinker CJ, Scherer GW. Sol-gel science: the physics and chemistry of sol-gel processing. Elsevier Inc. 2013;908. https://doi.org/10.1016/C2009-0-22386-5
18. Rajivgandhi GN, Ramachandran G, Kanisha CC, Alharbi NS, Kadaikunnan S, Khaled JM, *et al*. Effect of Ti and Cu doping on the structural, optical, morphological and anti-bacterial properties of nickel ferrite nanoparticles. Results Phys. 2021;23:104065. https://doi.org/10.1016/j.rinp.2021.104065
19. Virlan C, Bulai G, Caltun OF, Hempelmann R, Pui A. Rare earth metals' influence on the heat generating capability of cobalt ferrite nanoparticles. Ceram Int. 2016;42(10):11958-11965. https://doi.org/10.1016/j.ceramint.2016.04.121
20. Wang Y, Niu Z, Han H, *et al*. Observation of structural, mechanical, thermal and microwave dielectric properties of carbon black reinforced PA6/HDPE nanocomposites. J Mater Sci Mater Electron. 2023;34:1948-1958. https://doi.org/10.1007/s10854-023-11360-3
21. Zipare KV, Bandgar SS, Shahane GS. Effect of Dy-substitution on structural and magnetic properties of MnZn ferrite nanoparticles. J Rare Earths. 2018;36(1):86-94. https://doi.org/10.1016/j.jre.2017.06.011